IMAV2017-25
http://www.imavs.org/pdf/imav.2017.25

Bio-inspired Wind Field Estimation-Part 1: AoA Measurements Through Surface Pressure Distribution

Nikola Gavrilović*
Institut Supérieur de l'Aéronautique et de l'Espace-SUPAERO, Toulouse, 31400, France
Murat Bronz‡
l'Ecole National de l'Aviation Civile-ENAC, Toulouse, 31055, France
Jean-Marc Moschetta†, Emmanuel Bénard⊥and Philippe Pastor△
Institut Supérieur de l'Aéronautique et de l'Espace-Supaéro, Toulouse, 31400, France

ABSTRACT

One of the major challenges of Mini-UAV flight is unsteady interaction with turbulent environment while flying in lower levels of atmospheric boundary layer. Following inspiration from nature we expose a new system for angle of attack estimation based on pressure measurements on the wing. Such an equipment can be used for real-time estimation of the angle of attack during flight or even further building of wind velocity vector with additional equipment. Those information can find purpose in control and stabilization of the aircraft due to inequalities seen by the wing or even for various soaring strategies that rely on active control for energy extraction. In that purpose flying wing UAV has been used with totally four span-wise locations for local angle of attack estimation. In-flight angle of attack estimation of differential pressure measurements have been compared with magnetic sensor with wind vane. Difference in local angle of attack at four span-wise locations has confirmed spatial variation of turbulence. Moreover, theoretical energy dissipation of wind fluctuations described by Kaimal spectrum has shown acceptable match with measured ones.

1 INTRODUCTION

There are strong indications that birds use their feathers for sensing of flow perturbations over their wingspan. Being fluffy and subjected to fluttering provoked by small disturbances, birds have natural sensory system which enables them to "feel" flow disorders along wing. Another convenience of their elastic body structure is capability of using adaptronics for various turbulent flight regimes. Eventual immediate action due to surface pressure fluctuations by modifying wing geometry or profile curvature allows quick and effective response in gusty environment.

However, for a variety of reasons, it is understood that identical copies from nature to man-made technologies are not feasible. Instead, a creative inspiration and conversion into technology is often based on various steps of abstraction.

Mini UAVs usually fly at lower levels of atmospheric boundary layer where the turbulence intensity is significantly increased due to the proximity of the ground. Such a complex surrounding implies intricate interaction between terrains geometry, physical conditions and varying meteorology. Being three-dimensional, turbulence scales larger than wingspan would result in only pitching attitude of the aircraft. In contrary, case of turbulence smaller than wingspan leads to unequal lift distribution and need for control of oncoming roll and yaw moments. These information can be of particular interest in case of gust energy extraction flight strategy.

The performance of small UAVs being constrained by onboard energy due to their limited size can be significantly enhanced by specific flight strategies according to expected atmospheric formations. Most of the energy harvesting methods rely on active control system that detect and exploit the energy of atmospheric turbulence through intentional maneuvering of the aircraft. As a response for such a request this paper propose one of the methods for wind estimation which could be used as a direct input of control for energy harvesting strategy. Moreover, such a system could be replicated on various positions along wingspan which could provide necessary information on gust length scales during the flight. The major benefit of such a biologically inspired sensory system is that the flying vehicle senses the disturbances rather than its responses to it.

An approach based on Unscented Kalman Filter (UKF) is proposed by Condomines [1] for non-linear wind estimation in aspect of formation detection of cumulus-type clouds with a fleet of drones. Review and suitability of conventional sensors applicable to small UAVs is performed by Mohamed [2]. The use of pressure sensors on the wing as a stabilization system of a micro UAV for roll axis was demonstrated by Mohamed [3, 4]. Another way of stabilizing a small UAV

*PhD Candidate, Department of Aerodynamics, Energetics and Propulsion, (nikola.gavrilovic@isae.fr)
‡Assistant Professor, Applied Aedrodynamics URI-Drones
†Full Professor, Department of Aerodynamics, Energetics and Propulsion
⊥Associate Professor, Department of Conceptual Design of Aerospace Vehicles
△Associate Professor, Department of Conceptual Design of Aerospace Vehicles

in turbulent conditions has been performed by Mohamed [5] with pitch probes (multi-hole probes) located on both sides of the wing. Both ways promise more effective stabilization of the aircraft when compared to conventional inertial systems. Moreover, a correlation between a single pressure tap on the wing and cord-wise integrated pressure coefficient was used for roll mitigation of oncoming turbulence by Marino [6, 7]. Capacitive strip sensors applied on the airfoil skin was demonstrated by Callegari [8]. A stabilization systems based on surface pressure measurements can be considered as feeling way of turbulence affecting aircraft. They promise more effective response as opposed to conventional approach of traditional systems based on inertial sensors. The systems previously mentioned replicate the function of feathers and hairs as shown in Figure 1. A flush air data system intended for wind vector sensing in dynamic soaring UAVs is presented in [9]. The system uses pressure holes on the aircraft nose-cone as inspiration from Wandering Albatross and Giant Petrel nostrils. As opposite to fluffy wing structures, some birds are also equipped with rigid sensory systems as explained in previous work. An overall view on biologically inspired aerodynamic structures and their purpose is explained by Rasuo [10].

The advantage of the principle proposed in this paper is capability to estimate the precise value of angle of attack on the arbitrary chosen locations on the wing. Those precise information can be further used for meteorological investigation or as an direct input of control for energy extraction flight strategies of soaring or powered flight. The system is particularly interesting for soaring strategies as it allows aircraft to feel upcoming disturbances. It also provides insurance that detected turbulent structures can be exploitable due to their magnitude frequency and length scale.

2 Existing Meteorological Knowledge of Atmospheric Boundary Layer

Mini and micro UAVs predominantly fly in the surface of atmospheric boundary layer, where turbulence is strongly influenced by surface conditions, both terrain and temperature. We can differentiate two type of sources affecting turbulent formation of atmosphere. Mechanical is caused by friction as air flow masses move over the earth surface. Appearance of gradients in velocity will induce the formation of shear layers. Those shear layers produce rotating air motions or eddies and their strength is directly proportional to the magnitude of air velocity. The other sources could be the roughness and natural obstacles that deflect air flows. On the other hand thermal turbulence is caused by buoyancy effects. Unequal heating of the ground provoked by the clouds or natural obstacles as cliffs, mountains and valleys generate large circulation systems called thermals, where warmer air have a tendency of climbing while being replaced by cold air from the bottom. Those thermal irregularities are actually magnifying vertical mixing caused by mechanical turbulence. These two distinct sources present obvious challenge to flight stability and control but they also provide the opportunity and energy source for soaring flight strategies.

The measurements of turbulence in lower part of atmospheric boundary layer (region influenced by the frictional effect of surface extending from surface up to the range of 100 up to 1000 m depending on the surface and climate conditions) is usually done at fixed mast locations near wind turbine stations. It is known that turbulence intensity increases nearing the ground, strongly influenced by the terrain, thus changing the conditions comparable with those at high altitudes. Designation of standard deviation T_i of fluctuating velocity σ_u divided by mean velocity $\overline{U_z}$ for different altitudes and terrains shows that inhabited areas have the highest T_i of up to 50%. Although fluctuations are mainly present in the horizontal plane, while vertical components are mainly reduced but still present in the last couple of meters.

The average magnitude of wind in Europe measured in the horizontal plane at 10m above ground followed over the period of 44 years (1957-2002) show a variation of 2-4 $\mathrm{m{\cdot}s^{-1}}$ depending on the exact location of region as presented in [11]. Recent experiments from Watkins [12] considered measurements of spatial variation in pitch angle and confirmed statement about spatial variation of turbulence magnitude.

Previously described environment satisfies possible scenario of MAV flight concerning both altitude and experienced wind conditions. Moreover, it proves that atmospheric influence on low altitude UAV flight is three-dimensional.

3 Inspiration from Nature

Various styles of flight could be noticed while bird-watching. According to [13] birds use several strategies of energy harvesting, which serve as an inspiration for all the current improvements in the field of UAV long endurance performance. Interaction of wind and obstacles such as buildings, hills or waves generates an ascending component of air motion. Many birds with knowledge of soaring techniques use these up-drafts to power their flight instead of wing flapping. In case of unequal heating of earth's surface provoked by ex. punctured cloud layer, implies uplift of hot air, known as thermal. Eagles, condors, vultures and many other large birds use these up-drafts with a technique called thermal soaring in order to extend their endurance while searching for a prey. Another example is sweeping flight within the gust pushed by the waves. Gulls and pelicans use these gusts to power their flight by flying along the wave cliffs. Gaining speed while wave slows down, they are able to pull up and glide to another wave where the process continues. Some birds such as kestrels, remain motionless above a point on the ground by flying into the wind at a speed equal to that of the wind. This technique is called wind hovering.

There is a dense network of nerves around feather follicles according to [14]. Feathers are actually connected to the follicles in the skin and they represent a very complex system

of muscles and nerves interconnected. Primary function of such an anatomical configuration is mechanoreception. Specialized feathers on the head and breast have been shown to act as indicators of wind speed and direction. It has been also found that birds have very sensitive nerve endings (Herbst corpuscles) in their skin which are able to detect very high frequencies of vibrations of more than 100 Hz. Severe turbulent flows will cause the feathers to vibrate and gyrate wildly. As the feathers are elevated by the air stream, mechanoreceptors increase their discharge frequency according to [15].

Micro-structures require much more attention because they serve a lot of functions. So far understanding of flight control in birds is very limited. The connection between the natural sensory system and motor pathways involved in complex movements in soaring flight strategies have not yet been fully understood.

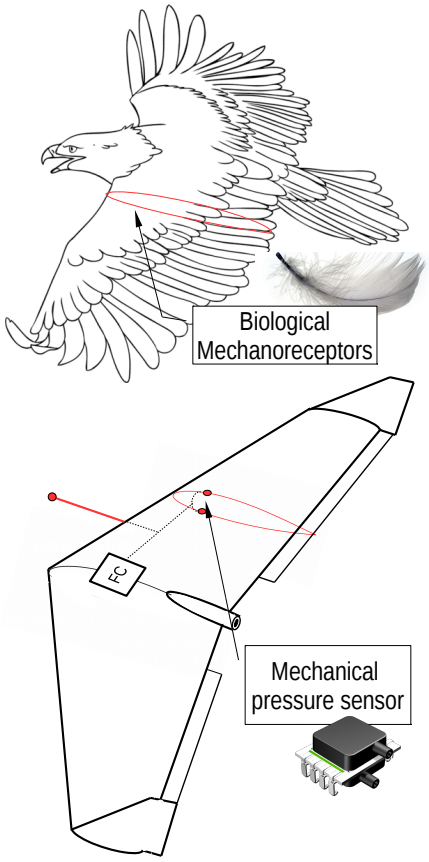

Figure 1: Bionical approach.

4 Algorithm Development

4.1 Wind Model for Simulations

From field experiments it is well known that undisturbed wind velocity is variable in space and time. The most adequate method to simulate a turbulent wind field would be to solve Navier-Stokes equations of an atmospheric flow bounded from below by an aerodynamically rough surface. This method requires enormous computational resources. Alternative could be Large Eddy simulations (LES) as an approximate solution to the Navier-Stokes equations where the smallest scales are not solved directly but modeled. Still even simplified alternative requires big computational power. Therefore, empirical description is generally used for turbulence representation, using spectral and coherence functions.

A model of turbulent wind field suitable for calculations requires good representation of both temporal and spatial structure of turbulence. Method for a generation of a single wind time series from a Kaimal spectrum is proposed by Branlard [16]. It leads to natural representation of turbulent flow of high computational cost compared to alternative Large Eddy or Navier-Stokes simulations. The spectrum used in simulations is presented by Kaimal [17] with its adjustable constants that depend on the chosen turbulent length scales, intensity of turbulence, surface roughness, Reynolds and Richardson number.

$$F_\alpha(k_1) = \frac{A \cdot \sigma_u^2 / k_{1m}}{1 + B \cdot (k_1/k_{1m})^{5/3}} \tag{1}$$

The characteristics of generated profiles are compared with available database on wind characteristics that can be found in [18] with intention to match the same level of turbulence energy (see Figure 2).

4.2 Numerical Calculations

After the generation of wind profile time series, two dimensional computational domain has been built with structured mesh around an airfoil SD2048. Structured mesh convergence has been studied previously to satisfy required number of cells for precise representation of boundary layer and wake formation. The chosen airfoil is a typical low-Reynolds number foil which could be found on several gliders including SB-XC used by NASA. The resulting vertical and horizontal wind profiles generated previously have been used as a direct input for inlet boundary condition of unsteady RANS simulations. The time step chosen for unsteady simulations was 0.5×10^{-4}s. The intention is to investigate the pressure variation on multiple locations of the airfoil and find a suitable way of achieving coherence with upcoming wind velocity or angle of attack. Moreover, the position of the pitot tube ahead of the airfoil was studied for various angles of attack.

The intention was to pick a specific pair of pressure ports where one port is on the upper surface of the airfoil and the other on the lower surface. Chosen pair has been selected with a request of precise estimation of angle of attack at high mean angles of attack, even after beginning of stall. Those points are recording a pressure with time, while the points in front of the airfoil record dynamic pressure (see Figure 3 for point location). The information on the pressure difference

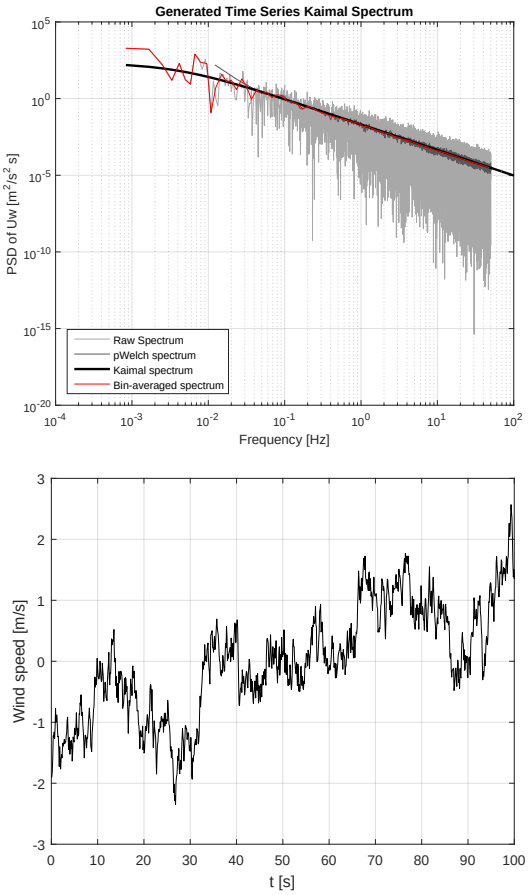

Figure 2: Generated time series of Kaimal spectrum as an input for URANS simulations.

is afterwards transformed into difference of pressure coefficients between the chosen ports. The following relation has been found:

$$\Delta C_{p12} = C_{p1} - C_{p2} = \frac{p_1 - p_2}{q} \tag{2}$$

The imposed wind profile at the inlet of the computational domain will generate additional angle of attack on the airfoil. The idea is to capture the angle of attack increments provoked by wind with related pressure coefficient fluctuations on the airfoil. This is achieved with polynomial fitting, where the optimization of the coefficients is performed with method of least squares.

$$\alpha = C_0 + C_1 \cdot \Delta C_{p12} + C_2 \cdot \Delta C_{p12}^2 \tag{3}$$

The relation claims that we are able to estimate the angle of attack knowing the pressure difference between the upper and lower point on the airfoil and dynamic pressure as shown in Figure 4. Once optimized for a certain airfoil and position of ports, coefficients of fitting were tested with various mean angles of attack and airspeeds. Those tests have shown that impact of Reynolds number variation does not affect significantly the angle of attack estimation.

However, for a variety of reasons it is clear that numerical simulations if posed correctly represent idealistic case where all the information of the flow are known in every node of the domain. Therefore, we proceed to realistic study of equipment in the flight test.

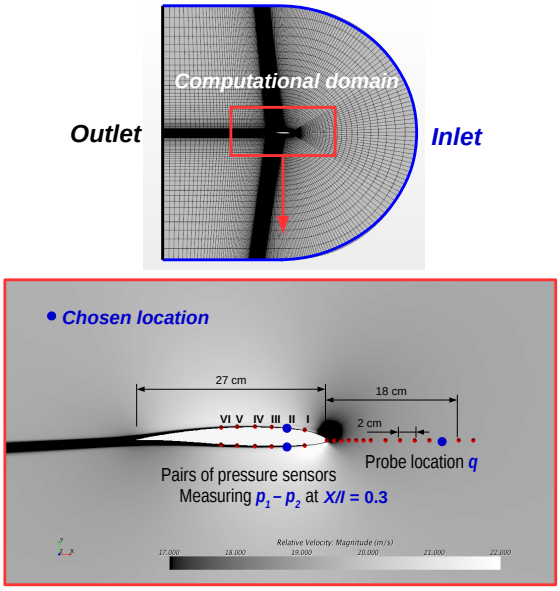

Figure 3: CFD computational domain of SD2048 Airfoil with port pair measuring pressure difference and pitot tube measuring dynamic pressure.

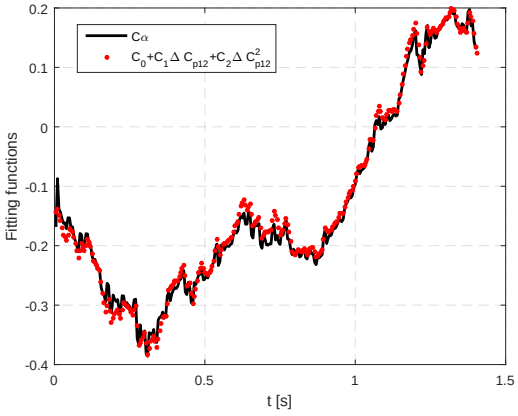

Figure 4: Curve fitting for numerical simulations ($Re = 340,000$).

5 PLATFORM

5.1 UAV and Equipment

The chosen flight test vehicle was a flying wing shown in Figure 5 built in UAV laboratory of ENAC. Particular interest of using flying wing configuration is sufficient thickness of the wing cord for sensor and equipment integration.

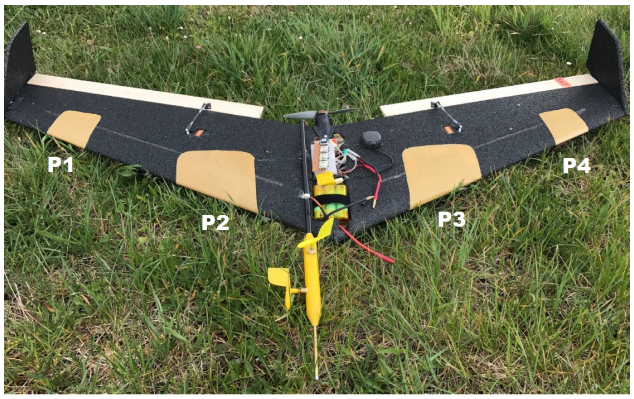

Figure 5: Flying wing UAV with equipment for angle of attack estimation.

Description	Details
Airfoil	Sipkill 1.7/10
Wingspan	1.2 m
Mean Aerodynamic cord	0.27 m
Weight	0.8 kg
Cruise speed	12 m/s
Aspect ratio	7

Table 1: Aircraft characteristics.

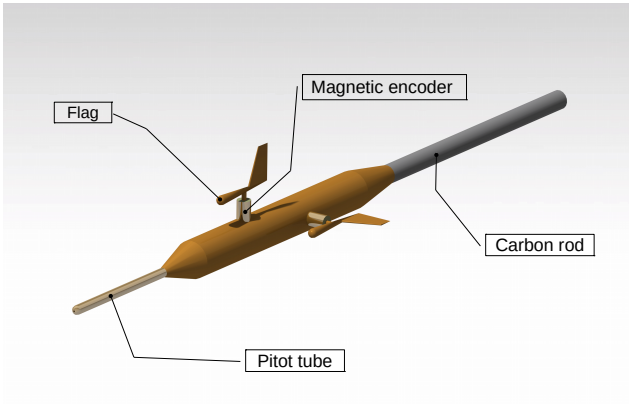

Figure 6: Pitot tube and wind vane with magnetic encoder.

Pressure sensors are located beneath the kevlar wing skin at 30% of cord distance. Small holes of 2mm diameter were made in vertical plane of the wing. Totally four places were chosen marked as points 1,2,3 and 4 on Figure 5. The distance between points is 40 cm. Each port pair is connected to a single differential pressure sensor.

Carbon rod has been joined to a 3d printed housing on its tip. The size of the housing was designed in a way to accept magnetic encoder, pitot tube and all necessary wiring and pressure tubes (see Figure 6). The length of the carbon rod was previously determined in CFD simulations for a non-disturbed pressure field condition. Small, 3d printed flag was attached to magnetic encoder. All of the sensors shown in Table 2 work at high frequency of 50Hz and recorded to on-board data logger except the differential GPS which works at 5 Hz.

Description	Details
Autopilot	Paparazzi [19] Chimera v1.0
IMU	MPU-9150 based
DGPS	NEO-M8P2
Differential pressure sensor	HCLA02×5EB
Magnetic Encoder	MA3-P12-125-B
Wind vane	3D printed
Pitot tube	10 cm

Table 2: Equipment on-board.

5.2 Calibration of Sensors

Calibration of the pitot tube, pressure sensors and the magnetic encoder has been performed in a wind tunnel with an autopilot on-board. Reference for pitot tube was imposed velocity of the wind tunnel measured with a hot wire anemometer. Calibration of pressure and flag sensor was done with respect to the IMU output from the autopilot, due to the equality of climb angle and angle of incidence in the wind tunnel. Curve fitting has been performed once again with least square method in PYTHON and obtained constant coefficients were used for further flight tests analysis. One of the drawbacks of this system is that pressure sensor (for angle of attack estimation) calibration is strictly related to the wing geometry of the pressure port location. Once calibrated, sensor for chosen aircraft and position is not reusable for a different wing shape and dimensions. Due to the required precision, ground and climb speed estimation could not rely on only GPS output. Especially problematic estimation of altitude requires combined work of barometer, differential GPS and accelerometer.

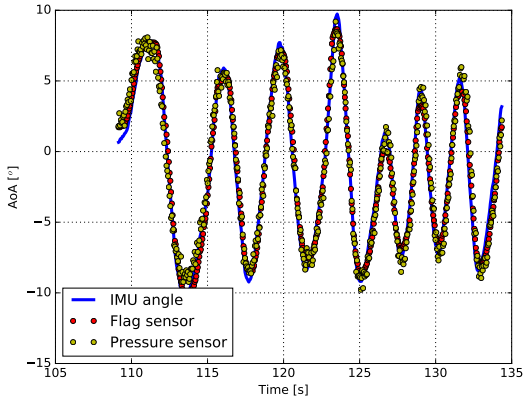

Figure 7: Results of calibration from wind tunnel experiment

6 Analysis of Experimental Data

6.1 Flight Data

Our intention is to use available information of flight parameters for further processing and transformation into wind components. The process of wind estimation requires knowledge of climb angle θ coming from IMU system, angle of attack α coming from pressure or flag sensors, dynamic pressure q coming from pitot tube and finally ground and climb speed coming from GPS, barometer and accelerometer combined together. With respect to the Figure 8 we write following equations for wind field estimation:

$$w_x = \dot{x}_i - V\cos\gamma \tag{4}$$

$$w_z = \dot{z}_i + V\sin\gamma \tag{5}$$

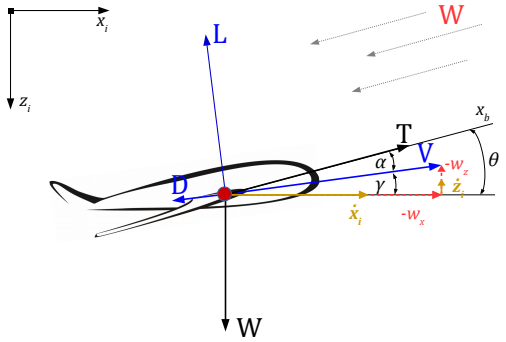

Figure 8: Longitudinal equations of motion.

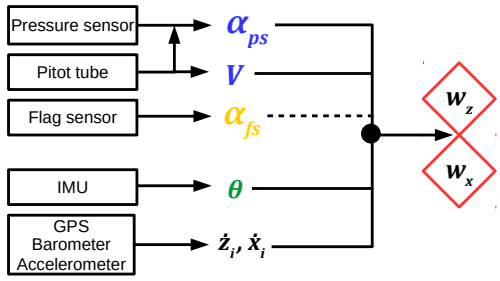

Figure 9: Algorithm for wind components estimation.

The flight has been started directly in autopilot assisted mode. After a short attempt, a small angle of attack increment was required in order to sustain the level flight. Due to the fact that ailerons occupy most of the wingspan, certain modifications in algorithm function have been made taking into account aileron deflection.

$$\alpha = C_0 + C_1 \cdot \Delta C_{p12} + C_2 \cdot \Delta C_{p12}^2 + C_3 \cdot \delta_a \tag{6}$$

Some intentionally provoked oscillations were made in order to visualize similarity between the angle of attack estimated by pressure and flag sensors. The following Figure 10 shows acceptable similarity between the two with a slight difference in magnitude. The difference is coming due to the fact that 3D printed flag has a certain inertia and due to rapid changes in angle of attack it shows a small increment.

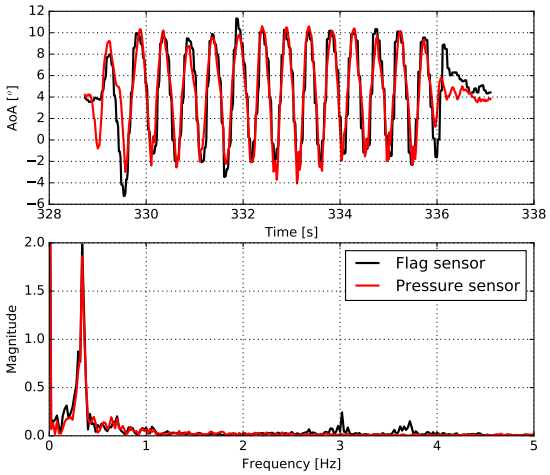

Figure 10: High frequency oscillations in flight test provoked by command input in calm atmosphere

Most of the time, flight test resulted with negligible error between angles estimated by different point locations (See

Figure 11). This is due to the fact that flying was conducted in relatively calm atmosphere with airspeed of 12 m/s. However, there were some parts where error was considerable. One of them is shown in Figure 12 where relative difference computed with respect to point 1 located at far right side of the wing is highest for point 4 located at opposite side of the wing. Described discontinuity results in roll and yaw moment regulated by actuators for autonomous flight regime. The discontinuity is coming from the small length scale gust, thus implying different wind components seen by each side of the wing locally. It is clear from Figure 12 that left side of the wing (Points 3 and 4) saw higher vertical wind component as this part of the wing registered higher local angle of attack. Locally, angle of attack were dropping till Point 1 with lowest amplitude.

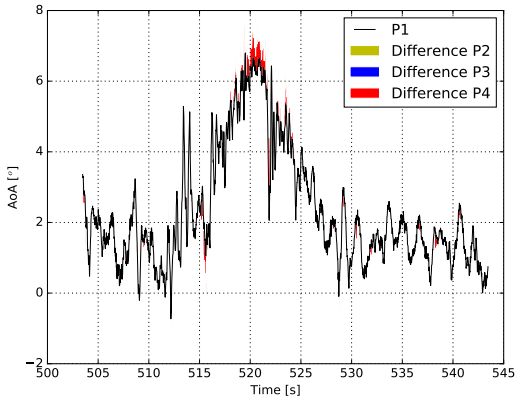

Figure 11: Local AoA difference compared to first point

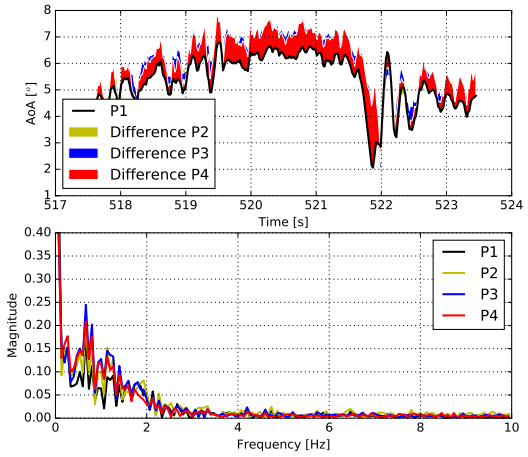

Figure 12: Local AoA difference compared to first point - zone of low coherence

Input for the control stabilization in this case is regulated from the IMU coming from autopilot. On one side, IMU acts as a correcting system which responds to direct consequence of disturbance, while on the other local angle of attack estimation promise "feeling" of upcoming disturbance pointing towards more effective way of control.

Advantage of having multiple location angle of attack sensors can also be found in stall control and evasion which was demonstrated by Bunge [20].

The following flight case can be divided into three phases. First phase represents partial stall of the right side of the wing as points 1 and 2 first reached stall limit. This led to an immediate, unrecoverable spin of the aircraft. Despite the efforts of autopilot to recover the plane, as he was leaving stall several short periods, right part of the wing was still reaching stall limit which resulted in a crash. The potential of these information could be easily implemented into the autopilot control laws, restricting the exceeding of stall limit on any part of the wing.

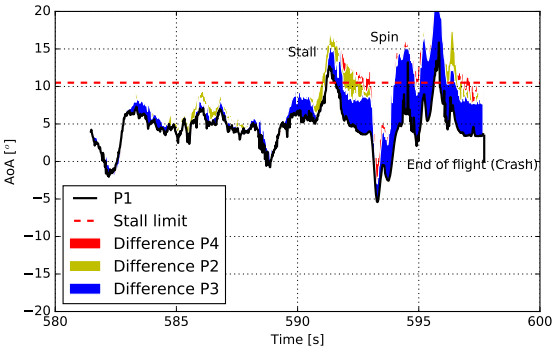

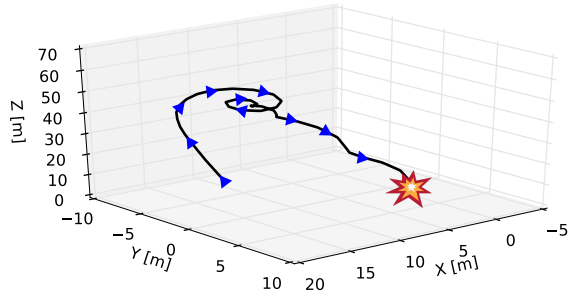

Figure 13: Stall, spin and crash

Moreover, the case of wind field estimation used as a control input for gust energy-extracting strategy can be a decisive mechanism for control activation as energy retrieval presented by Gavrilovic [21] is guaranteed in case of length scales greater than plane. Accurate estimation of wind field components depends on precision of all the elements involved as discussed in the beginning of this section. So far the estimation relies on available equipment where the weakest link

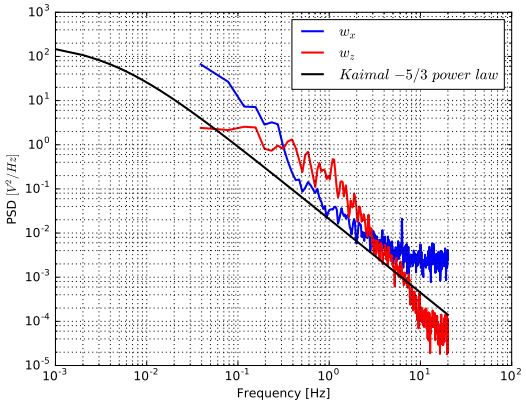

Figure 14: Estimated wind spectrum

is certainly the climb speed estimated by GPS. As shown in Figure 14 both vertical and horizontal component follow the natural law of turbulence dissipation represented by Kaimal spectrum [17] in this case. However, convincing statement on accuracy of wind components estimation requires comparison between estimated wind field by plane and available data from another source (example of flying around meteorological mast at different altitudes) which will be the subject of our further study.

7 Conclusion

Unlike the majority of the wind field data sets, the tests presented here are related to a typical mini UAV flying environment in the low-level of atmospheric boundary layer. The presented work shows development of a system for angle of attack estimation based on pressure measurements on the wing for further investigation of meteorological conditions experienced by a small UAV. The system showed several potential applications. The current results have concentrated on the spatial variation in angle of attack along an aircraft wing span. Ability to locally estimate the angle of attack promise potential for control of upcoming roll motions of the plane before the inertial response, as information on local angle of attack can be used as direct input of active control for stabilization. The difference between the local angles of attack have been clearly identified during the flight tests. Moreover, the system can be involved in a stall prevention mechanism of the autopilot. As critical point of stall on the wing depends on its geometry, those locations were used for pressure ports, thus detecting initial separations. Particular interest will be the implementation of algorithm for wind field estimation. Beside the knowledge of wind field components, the system will also provide a decisive mechanism for actions for power gain in energy harvesting flight strategies. Results have also shown acceptable comparison of measured and theoretical wind spectra.

Acknowledgements

Part of the presented UAS operations have been conducted at the Lannemezan experimental site belonging to the Pyrenean Platform of Observation of the Atmosphere (P2OA, hhtp://p2oa.aero.obs-mip.fr), a research platform of the University Paul Sabatier, Toulouse (France).

References

[1] Condomines, J-P., Bronz, M., Hattenberger, G. and Erdelyi, J-F., " Experimental Wind Field Estimation and Aircraft Identification," IMAV 2015, 2015.

[2] Mohamed, A., Clothier, R., Watkins, S. and Abdulrahim, M., "Fixed-wing MAV Attitude Stability in Atmospheric Turbulence, Part 1: Suitability of Conventional Sensors", *Progress in Aerospace Sciences*, 70, 2014.

[3] Mohamed, A., Watkins, S., Clothier, R. and Abdulrahim, M., "Influence of Turbulence on MAV Roll Perturbations," *International Journal of Micro Air Vehicles*, Vol 6, Number 3, 2014.

[4] Mohamed, A., Watkins, S., Fischer, A., Marino, M., Massey, K. and Clothier, R., "Bioinspired Wing-Surface Pressure Sensing for Attitude Control of Micro Air Vehicles," *Journal of Aircraft*, 2015.

[5] Mohamed, A., Abdulrahim, M., Watkins, S. and Clothier, R., "Development and Flight Testing of a Turbulence Mitigation System for Micro Air Vehicles," *Journal of Field Robotics*, 1-22, 2015.

[6] Marino, M., Watkins, S., Sabatini, R. and Gardi, A., "Unsteady Pressure Measurements on a MAV Wing for the Design of a Turbulence Mitigation System," IEEE, 2014.

[7] Marino M., "Unsteady Pressure Sensing on a MAV Wing for Control Inputs in Turbulence," PhD thesis, RMIT University, 2013.

[8] Callegari, S., Tallameli, A., Zagnoni, M., Golfarelli, A., Rossi, V., Tartagni, M. and Sangiorgi, E., "Aircraft Angle of Attack and Air Speed Detection by Redundant Strip Pressure Sensors", Sensors, IEEE, 2004.

[9] Quindlen, F. and Langelaan, J., "Flush Air Data Sensing for Soaring-Capable UAVs," AIAA 51st Aerospace science meeting, Grapevine, TX, USA, 2013.

[10] Rasuo, B., "Flight Mechanics," Faculty of Mechanical Engineering, University of Belgrade, Belgrade, (in Serbian) e-book, 2014.

[11] Peter, K., "Analysis of the European Wind Power Climatology and the Possible Cosmic Radiation Forcing on Global Lightning Activity," PhD Thesis, Budapest, Hungary, 2009.

[12] Watkins, S., Milbank, J., Loxton, B. and Melbourne, W., "Atmospheric WInds and Their Implications for Microair Vehicles," *AIAA Journal*, Vol. 44, No 11, 2006.

[13] Scott, S. and McFarland C., "Bird Feathers - A Guide to North American Species," Stackpole Books, 2010.

[14] Videler, J., "Avian Flight," Oxford Ornithology Series, Oxford University Press, New York, 2005.

[15] Brown, R. and Fedde R., "Airflow Sensors in the Avian Wing," *Journal of Experimental Biology*, 179, 13-30, 1993.

[16] Branlard, E., "Generation of Time Series From a Spectrum: Generation of Wind Time Series From the Kaimal Spectrum, Generation of Wave Time Series From Jonswap Spectrum," Technical University of Denmark, 2010.

[17] Kaimal, C. and Finnigan, J., "Atmospheric Boundary Layer Flows, Their Structure and Measurement", Oxford University Press, New York, 1994.

[18] Database on wind characteristics (online database), Dept. of Wind Energy, Technical Univ. of Denmark, Lyngby, Denmark, *winddata.com*.

[19] Hattenberger G., Bronz M. and Gorraz M., "Using the Paparazzi UAV System for Scientific Research," IMAV 2014, International Micro Air Vehicle Conference and Competition, 2014.

[20] Bunge, R., Alkuardi, A., Alfaris, E. and Kroo I., " In-Flight Measurement of Wing Surface Pressure on a Small-Scale UAV During Stall/Spin Maneuvers," AIAA Flight Testing Conference, Washington D.C., USA, 2016.

[21] Gavrilovic, N., Benard, E., Pastor, P. and Moschetta, J-M., "Performance Improvement of Small UAVs Through Energy Harvesting Within Atmospheric Gusts," Atmospheric Flight Mechanics Conference , Grapevine, TX, USA, 2017.